SUPPORTING INFORMATION

The influence of silica surface groups on the Li-ion conductivity of $LiBH_4/SiO_2$ nanocomposites

Peter Ngene[1#], Sander F. H. Lambregts[1], Didier Blanchard,[2] Tejs Vegge,[2] Manish Sharma,[3,4] Hans Hagemann,[3] and Petra E. de Jongh[1#]

[1)] Inorganic Chemistry and Catalysis; Debye Institute for Nanomaterials Science; Utrecht University, Utrecht, The Netherlands
[2)] Department of Energy Conversion and Storage; Technical University of Denmark, Roskilde, Denmark
[3)] Département de Chimie Physique; Université de Genève, Genève, Switzerland
[4)] Dept. Of Chemistry and Waterloo Institute of Technology, University of Waterloo, Waterloo, Ontario, Canada
[#] Corresponding authors : P.E.deJongh@uu.nl and P.Ngene@uu.nl

Contents: **page:**

Section 1 – Structural properties

Figure S1. Scanning electron micrograph of SBA-15 SiO_2-2 sputter coated with a 5 nm Pt. The image was recorded on a FEI XL30SFEG operating at 5 kV and measuring secondary electrons.

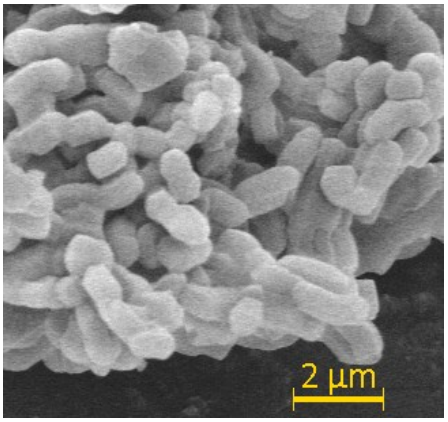

Figure S2. N_2 physisorption isotherms of the three batches of SBA-15 scaffolds used as a base for the experiments in this paper.

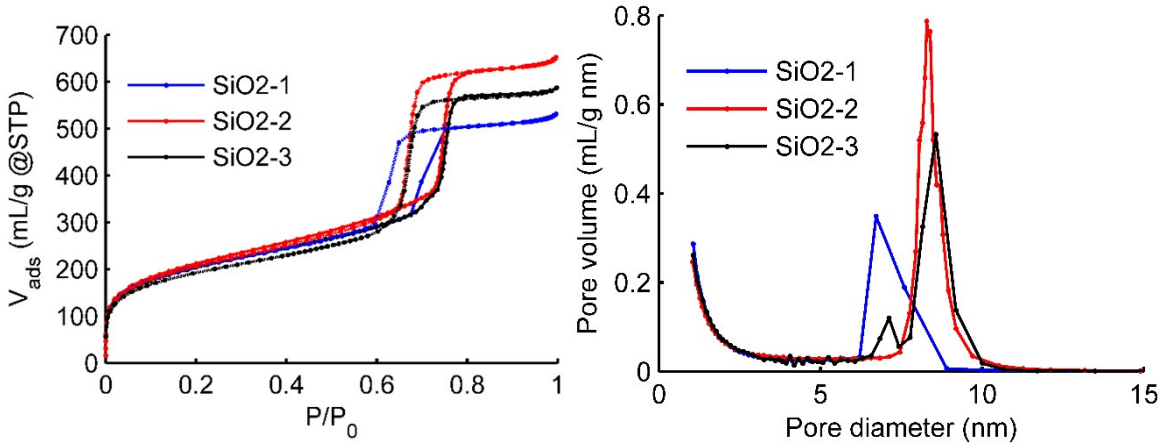

Table S1. BET surface area and constant, average mesopore diameter as derived from the adsorption isotherm pore volumes of the three batches of SBA-15 (SiO_2-1, SiO_2-2, and SiO_2-3) dried at 300 °C derived from the N_2 physisorption isotherm data represented in Figure S2. The micropore volumes were calculated using the t-plot method using the Harkins-Jura isotherm. The mesopore volumes $V_{mesopore}$ were calculated by using the t-plot method at a relative pressure higher than at which the hysteresis was observed and subtracting the micropore volume from the meso+micropore volume that was obtained from the extrapolated intercept of the y-axis in the t-plot. The pore diameter is taken as the pore size at which the maximum differential pore volume was found. The total pore volume was taken as the total volume of physisorbed nitrogen at p/p_0=0.997.

sample	A_{BET} m^2/g	C_{BET}	$d_{pore,BJH}$ nm	$V_{pore,\ total}$ cm^3/g	$V_{micropore}$ cm^3/g	$V_{mesopore}$ cm^3/g
SiO_2-1	744	150	7[1]	0.82	0.12	0.63
SiO_2-2	741	162	8.2	0.99	0.10	0.82
SiO_2-3	741	122	8.5	0.91	0.09	0.77

[1] too few points were taken in the relevant pressure range of the isotherm for an adequate pore size determination

Table S2: overview of the samples discussed in this paper; their denomination, from which SBA-15 batch they have been derived, and the amount of $LiBH_4$ added to form a nanocomposite using melt infiltration

sample name	SBA-15 batch no	Pretreatment temperature (in ^oC)	Amount of $LiBH_4$ (vol% wrt SiO_2 pore volume)
SiO_2-1-300	1	300	0
SiO_2-1-300-50	1	300	50
SiO_2-1-300-75	1	300	75
SiO_2-2-RT	2	(25)[1]	0
SiO_2-2-RT-100	2	(25)[1]	100
SiO_2-2-RT-130	2	(25)[1]	130
SiO_2-2-100	2	100	0
SiO_2-2-100-100	2	100	100
SiO_2-2-100-130	2	100	130
SiO_2-2-200	2	200	0
SiO_2-2-200-100	2	200	100
SiO_2-2-200-130	2	200	130
SiO_2-2-300	2	300	0
SiO_2-2-300-100	2	300	100
SiO_2-2-300-130	2	300	130
SiO_2-2-400	2	400	0
SiO_2-2-400-100	2	400	100
SiO_2-2-400-130	2	400	130
SiO_2-2-500	2	500	0
SiO_2-2-500-100	2	500	100
SiO_2-2-500-130	2	500	130
SiO_2-2-600	2	600	0
SiO_2-2-600-100	2	600	100
SiO_2-2-600-130	2	600	130
SiO_2-3-RT	3	(25)	0
SiO_2-3-RT-115	3	(25)	115
SiO_2-3-120	3	120	0
SiO_2-3-120-115	3	120	115
SiO_2-3-CH_3-115	3	120[2]	115
SiO_2-3-30	3	300	0
SiO_2-3-300-115	3	300	115
SiO_2-3-520	3	520	0
SiO_2-3-520-115	3	520	115
SiO_2-3-700	3	700	0
SiO_2-3-700-115	3	700	115

[1] dried in dynamic vacuum (roughly 1 mbar)
[2] Surface modified with trimethylsilyl

Table S3. Specific surface area, mesopore diameter and pore volumes of SiO_2-x (hydrothermal synthesis at 100 °C, subsequent heat treatment at different temperatures), determined using the adsorption isotherm of N_2-physisorption. The micro- and mesopore volumes were calculated using the t-plot method using the Harkins-Jura isotherm. The pore diameter was determined via the BJH model.

Sample	Heated to (°C)	A_{BET} m^2/g	C_{BET}	$d_{pore,BJH}$ nm	$V_{pore,\ total}$ cm^3/g	$V_{micropore}$ cm^3/g	$V_{mesopore}$ cm^3/g
SiO_2-2-100	100	732	173	8[1]	0.97	0.10	0.81
SiO_2-2-300	300	741	162	8[1]	0.99	0.10	0.82
SiO_2-2-500	500	750	160	8[1]	1.00	0.10	0.83
SiO_2-2-600	600	744	129	8[1]	0.98	0.09	0.84

[1] too few points were taken in the relevant pressure range of the isotherm for an adequate pore size determination

Section 2 – Electrochemical Impedance Spectroscopy results

Table S4. Impedance spectroscopy results of melt-infiltrated $LiBH_4/SiO_2$-2 nanocomposites. The apparent activation energy and pre-exponential factor in the low temperature phase were determined using the fits of the Arrhenius plots shown in figure 5 in the main paper. The correlation time is the inverse frequency at the apex of the arc in the Nyquist plot at 30±1°C.

Sample	Activation energy	Pre-exponential factor	Correlation time
	eV	10^4 S/cm	10^{-5} s
SiO_2-2-RT-130	0.62	2.0	5.2
SiO_2-2-100-130	0.57	0.9	3.9
SiO_2-2-200-130	0.57	1.6	1.3
SiO_2-2-300-130	0.58	1.7	1.6
SiO_2-2-400-130	0.57	2.1	2.4
SiO_2-2-500-130	0.62	5.4	1.4
SiO_2-2-600-130	0.56	0.8	1.8

Figure S3. Nyquist plots of SiO_2-2-300-130 at 30 and 90°C, and bulk $LiBH_4$ at 90°C (i.e. below its structural phase transition). To allow for direct comparison, each Nyquist plot has been scaled down by the corresponding ohmic resistance. All Nyquist plots show semicircles of comparable shape. Due to limitations on the frequency range of the instrument, the high frequency side (left side) of the semicircle is not always completely measured.

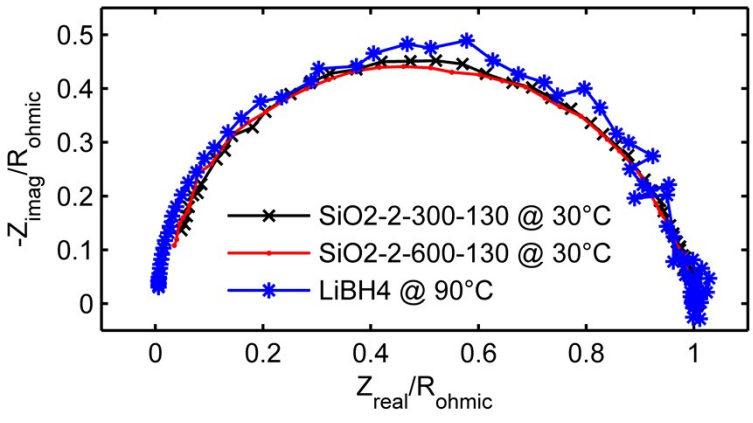

Figure S4. Arrhenius plots of the ionic conductivity as function of temperature for SiO_2-3-X-115 nanocomposites (SBA-15 SiO_2-3 heat treated at various temperatures in N_2 or at room temperature under vacuum after which a nanocomposite with $LiBH_4$ corresponding to 115% of the pore volume of the SiO_2 was prepared). Activation energies and pre-exponential factors were obtained (see Table S5) from a linear fit up to 105 °C. Also, the sample based on silylated SiO_2-3 is included.

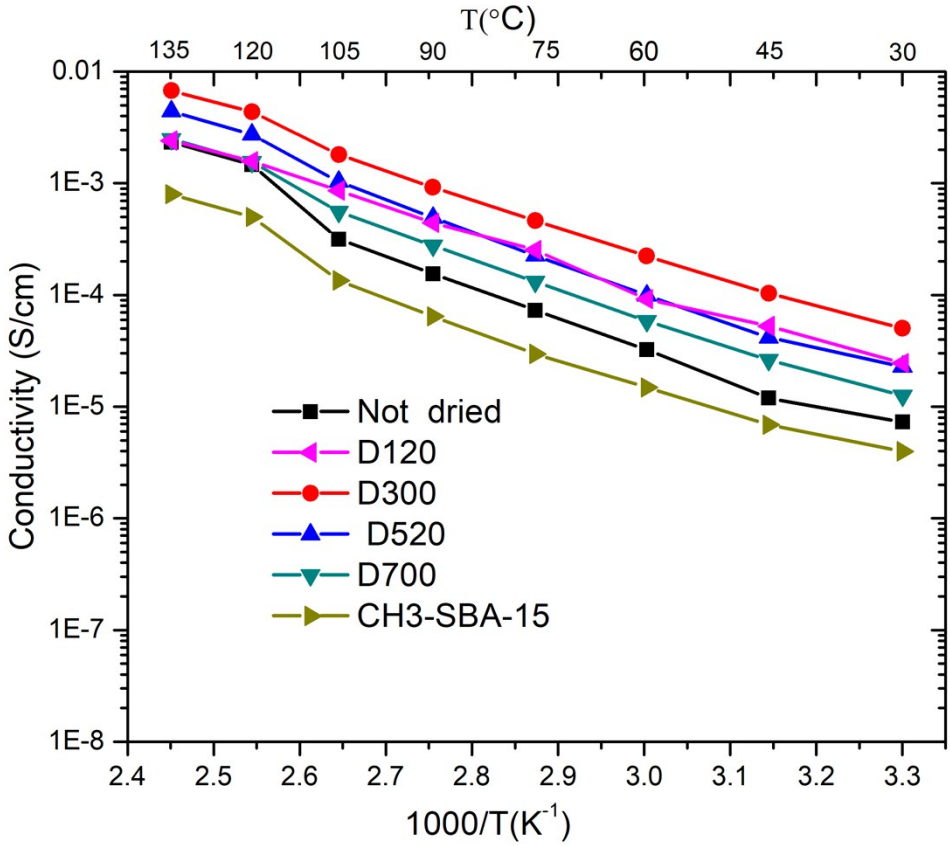

Table S5. Impedance spectroscopy results of melt-infiltrated $LiBH_4/SiO_2$-3 nanocomposites. The apparent activation energy and pre-exponential factor in the low temperature phase were determined using the fits of the Arrhenius plots shown in figure S4 just above. The correlation time is the inverse frequency at the apex of the arc in the Nyquist plot at 30 °C.

sample	activation energy	pre-exponential factor	correlation time
	eV	10^4 S/cm	10^{-5} s
SiO_2-3-RT-115	0.51	0.2	2.5
SiO_2-3-120-115	0.47	0.2	0.5
SiO_2-3-300-115	0.47	0.3	0.3
SiO_2-3-520-115	0.51	0.6	0.7
SiO_2-3-700-115	0.50	0.3	1.4

Figure S5. Comparison of the ionic conductivities of the nanocomposites SiO2-2-X-130 at 30°C measured at laboratories in Denmark (DTU) and in the Netherlands (UU). The measurement of SiO_2-2-300-130 measured at DTU was believed to be a very significant outlier, as it was not reproducible upon repeated measurement, hence it was omitted.

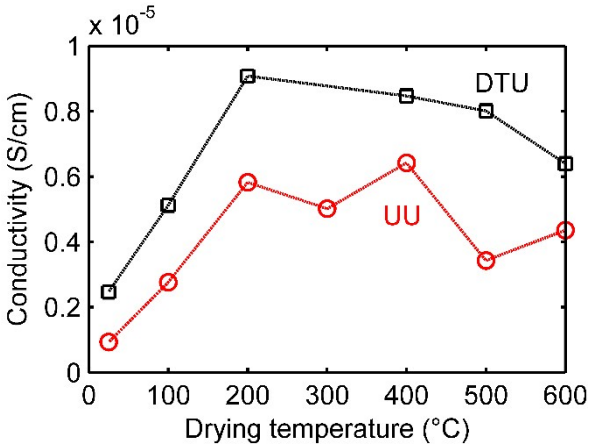

Section 3 – Detection of water for samples dried at low temperatures

Figure S6. Diffuse reflectance infrared spectra of SiO_2-2 SBA-15 prior to drying, after vacuum drying (in-situ dynamic vacuum) at room temperature and after drying for 6 hr at 100 °C under a flow of 25 ml/min N_2. Both vacuum drying and thermal drying at 100 °C remove some physisorbed water but vacuum drying alone is not likely to remove the silanol groups and water physisorbed/confined in the nanopores. The small additional peaks around 2800 and 1700 cm^{-1} in the vacuum dried sample is due to vacuum oil contamination of the sample during vacuum drying. Note that an offset in absorbance was applied for clarity.

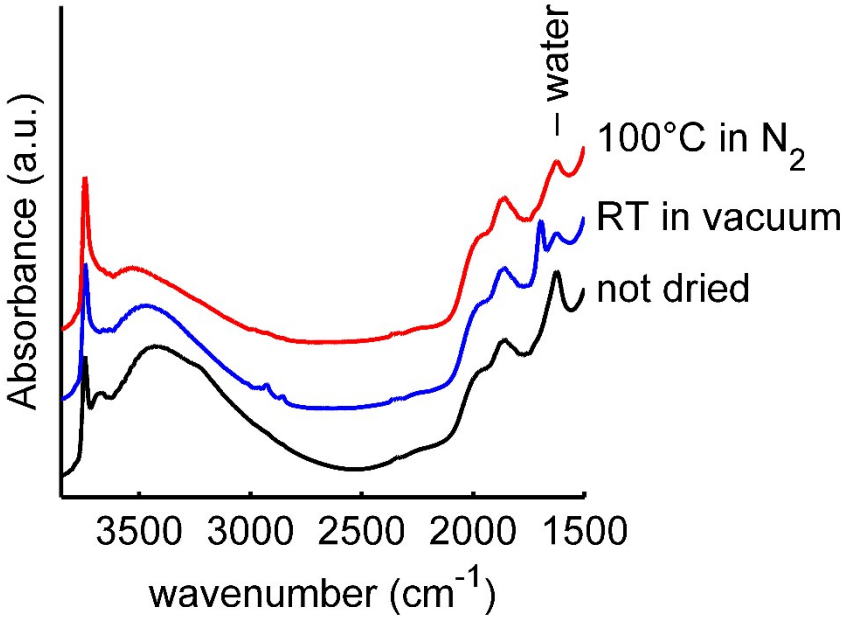

Section 4 - Determination of the SBA-15 pore filling via DSC and N_2 physisorption

Differential scanning calorimetry (DSC) and N_2-physisorption were used to estimate the extent to which the silica pores are filled with $LiBH_4$. From DSC, the amount of bulk-like $LiBH_4$ (hence outside the pores) can be determined, while N_2 physisorption on the other hand, shows how much of the SBA-15 porosity is lost due to incorporation of $LiBH_4$. Note that for the determination of the melt infiltration efficiency, an amount of $LiBH_4$ corresponding to 100 % of the silica pore volume was used in all the experiments.

Figure S7. Differential scanning calorimetry measurements showing the heat effects for pristine $LiBH_4$ and $LiBH_4$ confined SiO_2-2-300 at 300°C, with a theoretical $LiBH_4$ loading of 100 or 130% of the silica pore volume (i.e. SiO_2-2-300-100 and SiO_2-2-300-130). The properties of the SBA-15 SiO_2-2 are shown in table S1.

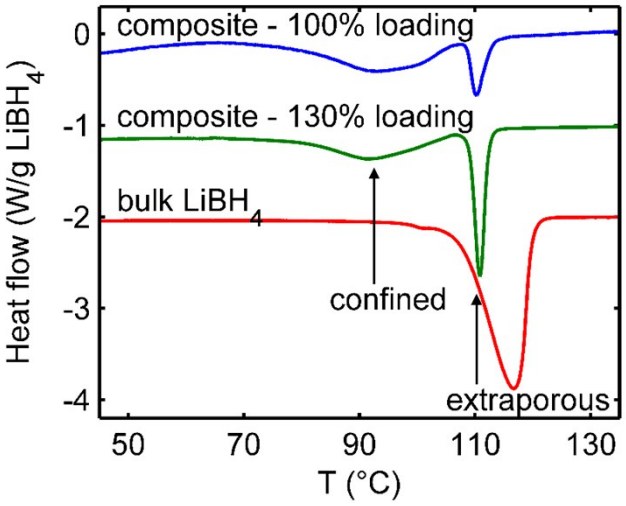

The DSC thermograms show the heat flow of $LiBH_4$ upon heating from 30 °C to 135 °C. In bulk $LiBH_4$, only a single, endothermic peak with an onset around 105 °C is present. This peak corresponds to the orthorhombic to hexagonal structural phase transition. For the nanocomposites, an additional endothermic peak is present at a lower temperature. This peak corresponds to $LiBH_4$ confined in the silica nanopores.[1-5] The peak due to macrocrystalline $LiBH_4$ is also visible, showing that some $LiBH_4$ did not enter the pores. At higher $LiBH_4$ loadings (volume or mass fraction), the integral of the bulk phase transition increases, which is expected because the volume of $LiBH_4$ exceeds the total pore volume of the silica. The pore filling, here denoted as η, can be calculated using formula (1). Here, V is the volume of *bulk* $LiBH_4$ or the silica pore volume (determined from N_2-physisorption), ($H^{o\rightarrow h}_{composite}$) is the measured enthalpy of the structural phase transition of the nanocomposite, while ($H^{o\rightarrow h}_{bulk}$) is that of the bulk or macrocrystalline $LiBH_4$ (-192 J/g)[6]. Note that the volume term is synonymous with the theoretical (expected) pore filling of the silica based on the amount (wt %) of $LiBH_4$ in the nanocomposite.

$$\eta^{DSC} = \frac{V^{LiBH_4}_{bulk}}{V^{silica}_{pore}}\left(1 - \frac{H^{o\rightarrow h}_{composite}}{H^{o\rightarrow h}_{bulk}\, wt\%}\right) \qquad (1)$$

Figure S8. N_2-physisorption isotherms of SiO_2-2 SBA-15 and nanocomposites SiO_2-2-X-100 that were pretreated at various temperatures. Note that each isotherm is normalized per gram silica, and all the nanocomposites contain an amount of $LiBH_4$ corresponding to a theoretical pore filling of 100 % (same volume as the total pore volume of the SBA-15).

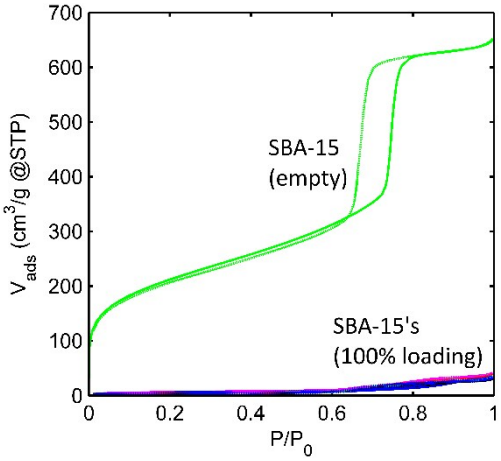

It can be seen that the hysteresis loop due to the mesopores is virtually absent in the nanocomposites, suggesting that almost all the mesopores are filled or blocked. However, some pore volume is left. Quantification of the total pore filling is based on the loss of pore volume of the silica, using formula (2). In this formula, *V* denotes the mesopore volume and *wt.%* the mass fraction of silica in the composite.

$$\eta^{phys} = 1 - \frac{V_{pore}^{composite}}{V_{pore}^{silica}\, wt\%} \qquad (2)$$

Section 5 – Effect of SiO_2-3 surface functionalisation

Figure S9. Diffuse reflectance infrared spectra of SiO_2-3 SBA-15 that was functionalized by treatment with chlorotrimethylsilane. In comparison with the non-modified SiO_2-2 SBA-15 (figure S6), new peaks corresponding to C–H stretching vibrations of the introduced methyl groups are clearly seen around 2900 cm^{-1}, showing that the silylation was successful. The presence of some vibrations corresponding to silanol groups is in line with the fact that the silylation procedure does not remove all the silanol groups.

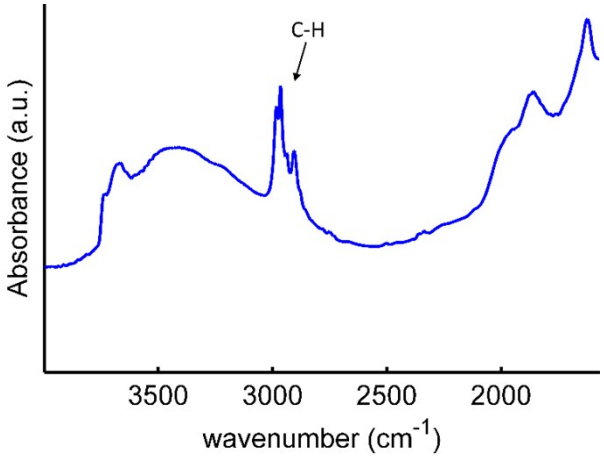

References

1. D. Blanchard, A. Nale, D. Sveinbjörnsson, T. M. Eggenhuisen, M. H. W. Verkuijlen, Suwarno, T. Vegge, A. P. M. Kentgens and P. E. de Jongh, *Advanced Functional Materials*, 2015, **25**, 184-192.
2. X. Liu, D. Peaslee, C. Z. Jost, T. F. Baumann and E. H. Majzoub, *Chemistry of Materials*, 2011, **23**, 1331-1336.
3. D. T. Shane, R. L. Corey, C. McIntosh, L. H. Rayhel, R. C. Bowman Jr, J. J. Vajo, A. F. Gross and M. S. Conradi, *The Journal of Physical Chemistry C*, 2010, **114**, 4008-4014.
4. S. Suwarno, P. Ngene, A. Nale, T. M. Eggenhuisen, M. Oschatz, J. P. Embs, A. Remhof and P. E. de Jongh, *The Journal of Physical Chemistry C*, 2017, **121**, 4197-4205.
5. N. Verdal, T. J. Udovic, J. J. Rush, X. Liu, E. H. Majzoub, J. J. Vajo and A. F. Gross, *The Journal of Physical Chemistry C*, 2013, **117**, 17983-17995.